Available online at www.sciencedirect.com
SCIENCE DIRECT®
Computer Vision and Image Understanding 101 (2006) 137–150
Computer Vision and Image Understanding
www.elsevier.com/locate/cviu

Multiregion competition: A level set extension of region competition to multiple region image partitioning

Abdol-Reza Mansouri [a], Amar Mitiche [b,*], Carlos Vázquez [b]

[a] Division of Engineering and Applied Sciences, Harvard University, Cambridge, MA 02138, USA
[b] INRS-EMT, University of Quebec, Place Bonaventure, Suite 6900, 800 de la Gauchetière West Montréal, Québec, Canada H5A 1K6

Received 8 March 2004; accepted 4 July 2005
Available online 11 October 2005

Abstract

The purpose of this study is to investigate a new representation of a partition of an image domain into a fixed but arbitrary number of regions by explicit correspondence between the regions of segmentation and the regions defined by simple closed planar curves and their intersections, and the use of this representation in the context of region competition to provide a level set multiregion competition algorithm. This formulation leads to a system of coupled curve evolution equations which is easily amenable to a level set implementation and the computed solution is one that minimizes the stated functional. An unambiguous segmentation is garanteed because at all time during curve evolution the evolving regions form a partition of the image domain. We present the multiregion competition algorithm for intensity-based image segmentation and we subsequently extend it to motion/disparity. Finally, we consider an extension of the algorithm to account for images with aberrations such as occlusions. The formulation, the ensuing algorithm, and its implementation have been validated in several experiments on gray level, color, and motion segmentation.

Keywords: Image segmentation; Motion segmentation; Image sequence analysis; Region competition; Curve evolution equations; Level set evolution equations

1. Introduction

Image segmentation is a fundamental problem in image processing and computer vision. It plays a central role in numerous useful applications such as satellite image analysis [1], biomedical image processing [2], scene interpretation [3,4], video image analysis [5,6], content-based image database retrieval [7], and many others.

With the introduction of active contours [8–11], various algorithms have been developed following formulations of segmentation as a Bayesian estimation problem or, more generally, as a functional minimization problem, where the solution is provided by evolution equations of closed simple plane curves. In general, these formulations are curve evolution implementation variants of the Mumford–Shah functional [12]. Some of these algorithms are contour-based [13–15], where curve evolution is guided solely by statistics on the active contours, while others are region-based [16–24], where statistics of regions—enclosed by the active contours—also contribute to curve evolution.

Whether contour-based or region-based segmentation formulations are difficult to extend beyond the two-region case of foreground and background using the standard correspondence between the regions of segmentation and the regions bounded by the curves. This standard correspondence leads to ambiguities in segmentation when the interior of two or more curves overlap, because region membership of points in the intersections is ambiguous. How to guarantee that the functional minimization results in a *partition* of the image domain is an important

* Corresponding author. Fax: +1 514 875 0344.
E-mail addresses: mansouri@deas.harvard.edu (A.-R. Mansouri), mitiche@inrs-emt.uquebec.ca (A. Mitiche), vazquez@inrs-emt.uquebec.ca (C. Vázquez).

1077-3142/$ - see front matter © 2005 Elsevier Inc. All rights reserved.
doi:10.1016/j.cviu.2005.07.008

question. We address explicitly the question in this paper. Current answers are the following:

(1) start with an initial partition into regions bounded by N closed simple curves γ_i and evolve $\Gamma = \cup\gamma_i$ according to a functional that references Γ as a curve that defines a partition. This is the approach adopted in [17]. Its implementation requires careful initialization and an explicit representation of Γ as a set of points on the image domain grid that does not accommodate changes in the topology of the curves during their evolution. The approach precludes the use of level sets since a single level set cannot represent a partition into more than two regions. The level set formalism is quite important in segmentation by active contours because it allows changes in the segmentation topology during curve evolution, and it is implementable by stable numerical schemes [25,26]. In this formalism, active contours are represented implicitly as zero level sets of functions over the image domain. Advantages of the level set representation of active contours over their explicit representation as a set of points, as with snakes, are generally acknowledged in gray-level image segmentation as well as motion segmentation and tracking [27–35],

(2) use a term in the functional that draws the solution towards a partition [22,21]. This does not guarantee a partition. Curve evolution will likely give an ambiguous segmentation if the partition constraint is not sufficiently enforced, and if it is strongly enforced, the curves will evolve more as a result of the partition constraint than of image statistics,

(3) use a functional that results in curve evolution equations where the evolution of a curve involves a reference to the others. This is the approach adopted in [24], referred to as a fully global approach. In this case, minimization of the functional results in a partition at convergence. However, the functional used in [24] is peculiar in the sense that a segmentation into N regions can be obtained only for vector images of dimension $N-1$ or higher. For instance, the functional cannot be used to segment an intensity image into more than two regions, unless it is filtered to be replaced by a vector valued image of intensity statistics [36,37]. Also, the observation term in the functional measures an $(N-1)$-dimensional volume. The complexity of the expression of this volume and of the corresponding terms in the Euler–Lagrange equations of minimization results in an excessive computational demand,

(4) generalize directly the curve evolution equations of the two-region case, rather than the functional itself. This is the approach adopted in [29]. This allows the use of non-differentiable operators that cannot be introduced in the functional, such as *min* or *max*, to express the competition for points between regions. This is a convenient, practical generalization although the computed solution looses its tie to the original functional,

(5) establish an explicit correspondence between the regions of segmentation and the regions defined by the curves and their intersections. This is the approach proposed in [20], also used for vector valued images in [23]. It guarantees a partition at all times during the curves evolution, and the computed solution is one that minimizes the original functional. Rather than for a fixed but arbitrary number of regions, the problem is stated for a number N of regions that is upper bounded by a power of 2, using $\log_2 N$ level set functions. Some of these regions can vanish, as shown on examples. Therefore, the method seeks a segmentation into up to a power of 2 number of regions. There is no clear indication on the actual number of regions the method yields since this depends not just on the image but also on the weight of the regularization term. In some instances, unwanted division of regions can occur, as with image segments of planar intensity variation.

The purpose of our study is to investigate a new representation of a partition of an image domain into a fixed but arbitrary number of regions by explicit correspondence between the regions of segmentation and the regions defined by simple closed planar curves and their intersections, and the use of this representation in the context of region competition [17] to provide a level set multiregion competition algorithm. The functional of this formulation leads to a system of coupled curve evolution equations which is easily amenable to a level set implementation, in contrast with the functional in [17] which precludes the use of level sets. It allows segmentation of images, scalar or vectorial, into a fixed but arbitrary number of regions, in contrast with the formulations in [24] which requires a vectorial image of dimension $N-1$ for segmentation into $N>2$ regions, and in [20] where the referenced number of regions of segmentation is a power of 2. The functional minimization guarantees an unambiguous segmentation because at all time during curve evolution the evolving regions form a partition of the image domain. This is due to a representation of an image partition in terms of evolving regions in such a way that any family of simple closed plane curves leads to an unambiguous segmentation. In contrast with [17,29] and others, the computed solution is one that minimizes the stated functional.

We provide a statement of multiregion competition for intensity-based segmentation. This is later extended to motion, and disparity-based segmentation to acknowledge explicitly the fact that the problem of segmenting intensity images is conceptually similar to the problem of segmenting motion or disparity fields, color images, and vector images of statistics of intensity. We also provide an extension of the multiregion competition algorithm which accounts, by an outlier rejection model, for distortions such

as occlusions. To validate the formulation, the ensuing algorithm and its implementation, we ran several experiments on gray level, color, and motion segmentation. With the experiment of motion-based image segmentation we highlight the difference in segmentation that is obtained with and without the extension for outliers rejection.

The remainder of this paper is organized as follows: Section 2 states the problem of image partitioning via curve evolution for intensity-based segmentation. Section 3 details the proposed representation of a partition into a fixed but arbitrary number of regions, the multiregion competition functional, the corresponding Euler–Lagrange curve evolution equations and their level set expression. In Section 4, the formulation is extended to motion/disparity segmentation. Section 5 discusses the extended image formation model. Section 6 describes an experimental verification, and Section 7 contains a conclusion.

2. Image partitioning via curve evolution

2.1. Basic models

Here following is a statement of the problem of image segmentation for intensity images. An extension to vectorial images, motion, and disparity-based segmentation will be presented later in a subsequent section.

Let $\mathbf{I} : \Omega \to \mathbb{R}^n$, be an intensity image function, with domain $\Omega \subset \mathbb{R}^2$. The goal of image segmentation is to obtain a *partition* of Ω from the image $\mathbf{I}$, that is, a family $\{\mathbf{R}_i\}_{i=1}^N$ of subsets of Ω which are pairwise disjoint and such that they cover Ω. Formulating segmentation as a Bayesian estimation problem, the segmentation estimate of maximum a posteriori probability $\{\mathbf{R}_i\}_{i=1}^N$ is given by:

$$\{\hat{\mathbf{R}}_i\}_{i=1}^N = \arg\max_{\{\mathbf{R}_i \subset \Omega\}} P(\mathbf{I}|\{\mathbf{R}_i\})P(\{\mathbf{R}_i\}),$$

where $P(\mathbf{I}|\{\mathbf{R}_i\})$ is the likelihood of the segmentation, and $P(\{\mathbf{R}_i\})$ its prior. The image formation can be modeled via a piecewise function, such that

$$\widetilde{\mathbf{I}} = \sum_{j=1}^{N} (\alpha_j + \mu_j)\chi_{\mathbf{R}_j}, \tag{1}$$

where $\chi_{\mathbf{R}_j}$ is the indicator function of the set $\mathbf{R}_j$, defined by $\chi_{\mathbf{R}}(\mathbf{x}) = 1$ (resp. 0) if $\mathbf{x} \in \mathbf{R}$ (resp. $\mathbf{x} \notin \mathbf{R}$), and μ_j is a stationary white Gaussian noise process with zero mean and covariance matrix Σ_j. In Eq. (1) $\alpha_j : \Omega \to \mathbb{R}^n$ is the restriction to region $\mathbf{R}_j$ of the noiseless image underlying the observed image, i.e., the observed image is an ideal noiseless image plus noise.

We will assume that the α_j are independent of the segmentation $\{\mathbf{R}_i\}$. We will also assume that the α_j are either computed prior to the segmentation, as in [21,29], for instance, or are computed iteratively as suggested in [17] in parallel with the segmentation. In both cases, the estimation of the α_j is a process separate from the segmentation itself, and because it is highly problem-dependent and well-studied, we will forego its inclusion here. In what follows, we shall therefore focus exclusively on the estimation of the segmentation $\{\mathbf{R}_i\}$, via curve evolution, and assume the α_j known.

The maximum a posteriori estimate $\{\hat{\mathbf{R}}_i\}_{i=1}^N$ of the segmentation then becomes:

$$\{\hat{\mathbf{R}}_i\}_{i=1}^N = \arg\max_{\{\mathbf{R}_i \subset \Omega\}} P(\widetilde{\mathbf{I}}|\mathbf{I}, \{\mathbf{R}_i\})P(\mathbf{I}|\{\mathbf{R}_i\})P(\{\mathbf{R}_i\})$$

and, assuming $\mathbf{I}$ is independent of the segmentation $\{\mathbf{R}_i\}$, we obtain

$$\begin{aligned}\{\hat{\mathbf{R}}_i\}_{i=1}^N &= \arg\max_{\{\mathbf{R}_i \subset \Omega\}} P(\widetilde{\mathbf{I}}|\mathbf{I}, \{\mathbf{R}_i\})P(\{\mathbf{R}_i\}) \\ &= \arg\max_{\{\mathbf{R}_i \subset \Omega\}} P\left(\sum_{j=1}^{N}(\alpha_j + \mu_j)\chi_{\mathbf{R}_j}|\mathbf{I}, \{\mathbf{R}_i\}\right)P(\{\mathbf{R}_i\})\end{aligned}$$

which in turn, leads to

$$\{\hat{\mathbf{R}}_i\}_{i=1}^N = \arg\max_{\{\mathbf{R}_i \subset \Omega\}} \left\{\left(\prod_{j=1}^{N}\prod_{\mathbf{x}\in\mathbf{R}_j} N(\mathbf{I}(\mathbf{x}) - \alpha_j, \Sigma_j)\right)P(\{\mathbf{R}_i\})\right\}$$

using independence of the noise process μ_j ($N(v, \Sigma)$ denoting the Gaussian with mean v and covariance matrix Σ), and finally, taking the logarithm of the right-hand side, this Bayesian estimation problem is converted to the following minimization problem:

$$\{\hat{\mathbf{R}}_i\}_{i=1}^N = \arg\min_{\{\mathbf{R}_i \subset \Omega\}} E[\{\mathbf{R}_i\}_{i=1}^N],$$

where the energy $E[\{\mathbf{R}_i\}_{i=1}^N]$ is defined by

$$E[\{\mathbf{R}_i\}_{i=1}^N] = \sum_{j=1}^{N} \int_{\mathbf{R}_j} \xi_j(\mathbf{x})\,d\mathbf{x} - \log P(\{\mathbf{R}_i\}) \tag{2}$$

and

$$\xi_j(\mathbf{x}) \equiv \tfrac{1}{2}\log|\Sigma_j| + \tfrac{1}{2}(\mathbf{I}(\mathbf{x}) - \alpha_j)^{\mathrm{T}}\Sigma_j^{-1}(\mathbf{I}(\mathbf{x}) - \alpha_j(\mathbf{x})),$$

where $|\cdot|$ denotes determinant.

2.2. Image partitioning via curve evolution

Consider a family $\vec{\gamma}_i : [0,1] \to \Omega,\ i = 1, \ldots, N-1$ of closed simple plane curves parametrized by the arc parameter $s \in [0,1]$. Typically, the maximum a posteriori estimation of the regions $\{\mathbf{R}_i\}$ is converted to a maximum a posteriori estimation of plane curves by associating to region $\mathbf{R}_j$ the region $\mathbf{R}_{\vec{\gamma}_j}$ inside the curve $\vec{\gamma}_j$, for all $j = 1, \ldots, N-1$, and to region $\mathbf{R}_N$ of the segmentation the complement $(\cup_{j=1}^{N-1}\mathbf{R}_{\vec{\gamma}_j})^c$ of the union of the $\mathbf{R}_{\vec{\gamma}_j}$ for $j = 1, \ldots, N-1$. This yields the following energy minimization problem:

$$\{\hat{\vec{\gamma}}_i\}_{i=1}^{N-1} = \arg\min_{\{\vec{\gamma}_i:[0,1]\to\Omega\}} E[\{\vec{\gamma}_i\}_{i=1}^{N-1}],$$

where

$$E[\{\vec{\gamma}_i\}_{i=1}^{N-1}] = \sum_{j=1}^{N-1}\int_{\mathbf{R}_{\vec{\gamma}_j}} \xi_j(\mathbf{x}) + \int_{(\cup_{j=1}^{N-1}\mathbf{R}_{\vec{\gamma}_j})^c} \xi_N(\mathbf{x}) - \log P(\{\vec{\gamma}_i\})$$

the minimization being performed by Euler–Lagrange curve evolution equations. The term $-\log P(\{\vec{\gamma}_i\})$ is usually taken to be a function of curve length such as

$$-\log P(\{\vec{\gamma}_i\}) = \lambda \sum_{j=1}^{N-1} \oint_{\vec{\gamma}_j} \mathrm{d}s. \tag{3}$$

For $N = 2$, i.e., in the case of two region (foreground/background) segmentation, this functional is identical to the region competition functional proposed in [17] for image segmentation, while for more than two regions, the functional obtained is identical to the extension proposed in [24] of the Chan–Vese functional [38]. The Euler–Lagrange descent equations of the functional thus obtained are given by embedding the family $\vec{\gamma}_i : [0,1] \to \Omega, i = 1,\ldots,N-1$, of plane curves into one-parameter families $\vec{\gamma}_i : [0,1] \times \mathbb{R}^+ \to \Omega, i = 1,\ldots,N-1$, of plane curves constructed by solving the following system of evolution equations:

$$\frac{\mathrm{d}\vec{\gamma}_j}{\mathrm{d}t} = -\frac{\delta E}{\delta \vec{\gamma}_j}, \qquad j = 1,\ldots,N-1,$$

where $\frac{\delta E}{\delta \vec{\gamma}_j}$ denotes the functional derivative of the energy functional E with respect to the curve $\vec{\gamma}_j$. The desired segmentation is given by the family $\{\mathbf{R}_{\vec{\gamma}_j}\}$ of regions obtained for $t \to \infty$.

The fundamental problem associated with this functional is that the family of regions obtained after solving the minimization problem does not generally form a partition of the image domain, for although the $\mathbf{R}_{\vec{\gamma}_j}$ together with $(\cup_{j=1}^{N-1}\mathbf{R}_{\vec{\gamma}_j})^c$ do cover the image domain Ω, the $\mathbf{R}_{\vec{\gamma}_j}$ may not be pairwise disjoint. This lack of pairwise disjointness leads in turn to ambiguity in the segmentation: it is not possible to decide to what region a point does belong. To alleviate this problem, it is possible to enforce the partition constraint by adding penalty terms to the energy functional to bias the solution of the energy minimization problem towards pairwise disjoint families of regions. Such penalty terms usually take the form of area integrals computed over intersections of distinct regions, such as

$$\frac{\lambda_P}{2} \sum_{i=1}^{N-1} \sum_{j \neq i} \int_{\mathbf{R}_{\vec{\gamma}_i} \cap \mathbf{R}_{\vec{\gamma}_j}} \mathrm{d}\mathbf{x}$$

and have been proposed in [21]. It is important to note that the system obtained here is a system of *coupled* evolution equations, the coupling reflecting the fact that the various plane curves interact to reduce their overlap. The problem with this approach is that the overlap problem is reduced but not totally eliminated, and the ambiguity in segmentation persists. Furthermore, modifying the energy functional by adding the overlap penalty terms may bias the solution of the original problem away from the intended solution, and may create excessive dependence on the coefficient λ_P.

3. Multiregion competition algorithm

3.1. Representation of a partition into a fixed but arbitrary number of regions: removing ambiguities

The ambiguity in segmentation described in the previous section can be eliminated altogether without the use of any penalty terms in the energy functional as in [23,21], by establishing a suitable correspondence between regions enclosed by closed simple plane curves and regions in the segmentation. This correspondence is key to the multiregion competition algorithm and guarantees that at all time the partition constraint is maintained. Consider a family $\vec{\gamma}_i : [0,1] \to \Omega, i = 1,\ldots,N-1$, of plane curves parametrized by the arc parameter $s \in [0,1]$. We propose the following correspondence between the family $\{\mathbf{R}_{\vec{\gamma}_i}\}$ of regions enclosed by the curves $\{\vec{\gamma}_i\}$ and the segmentation $\{\mathbf{R}_i\}$ of the image domain Ω: We associate to region $\mathbf{R}_1$ of the segmentation the region $\mathbf{R}_{\vec{\gamma}_1}$ inside the curve $\vec{\gamma}_1$, as in the standard case described in Section 2.2; to region $\mathbf{R}_2$ of the segmentation, however, we associate the region $\mathbf{R}^c_{\vec{\gamma}_1} \cap \mathbf{R}_{\vec{\gamma}_2}$ described by the plane curves, in sharp difference to the standard case; to region $\mathbf{R}_3$ of the segmentation, we similarly associate region $\mathbf{R}^c_{\vec{\gamma}_1} \cap \mathbf{R}^c_{\vec{\gamma}_2} \cap \mathbf{R}_{\vec{\gamma}_3}$, and continuing this construction, we associate to region $\mathbf{R}_k$ of the segmentation (for $k \leqslant N-1$) the region $\mathbf{R}^c_{\vec{\gamma}_1} \cap \mathbf{R}^c_{\vec{\gamma}_2} \cap \cdots \cap \mathbf{R}^c_{\vec{\gamma}_k - 1} \cap \mathbf{R}_{\vec{\gamma}_k}$ defined by the plane curves $\{\vec{\gamma}_i\}$, while region $\mathbf{R}_N$ of the segmentation is finally associated to the region $\mathbf{R}^c_{\vec{\gamma}_1} \cap \mathbf{R}^c_{\vec{\gamma}_2} \cap \cdots \cap \mathbf{R}^c_{\vec{\gamma}_{k-1}} \cap \mathbf{R}^c_{\vec{\gamma}_{N-1}} = (\cup_{j=1}^{N-1}\mathbf{R}_j)^c$, as in the standard case described in Section 2.2. The family $\{\mathbf{R}_{\vec{\gamma}_1}, \mathbf{R}^c_{\vec{\gamma}_1} \cap \mathbf{R}_{\vec{\gamma}_2}, \mathbf{R}^c_{\vec{\gamma}_1} \cap \mathbf{R}^c_{\vec{\gamma}_2} \cap \mathbf{R}_{\vec{\gamma}_3}, \ldots\}$ thus obtained is clearly a partition of the image domain, for any family of plane curves $(\vec{\gamma}_i)_{i=1}^{N-1}$. The partition representation is illustrated on four regions of segmentation (three curves) in Fig. 1.

3.2. Multiregion competition functional

With our choice of representation of a partition of the image domain into N regions, the definition of ξ in

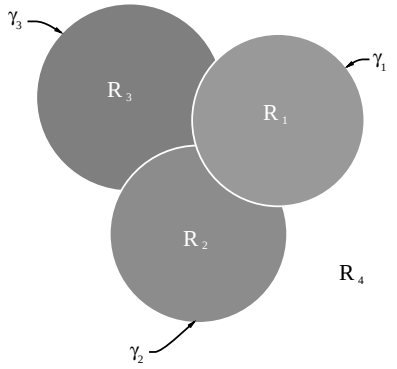

Fig. 1. Representation of a partition of the image domain by explicit correspondence between regions of segmentation and regions defined by closed simple planar curves (illustration for four regions).

Eq. (3) and with the prior term $-\log P(\{\vec{\gamma}_i\})$ as in Eq. (3), the energy functional Eq. (2) becomes:

$$\begin{aligned}E[\{\vec{\gamma}_i\}_{i=1}^{N-1}] = &\int_{\mathbf{R}_{\vec{\gamma}_1}} \xi_1(\mathbf{x})\,d\mathbf{x} + \int_{\mathbf{R}^c_{\vec{\gamma}_1}\cap\mathbf{R}_{\vec{\gamma}_2}} \xi_2(\mathbf{x})\,d\mathbf{x} + \cdots \\ &+ \int_{\mathbf{R}^c_{\vec{\gamma}_1}\cap\mathbf{R}^c_{\vec{\gamma}_2}\cap\mathbf{R}_{\vec{\gamma}_3}} \xi_3(\mathbf{x})\,d\mathbf{x} + \cdots \\ &+ \int_{\mathbf{R}^c_{\vec{\gamma}_1}\cap\mathbf{R}^c_{\vec{\gamma}_2}\cap\mathbf{R}^c_{\vec{\gamma}_3}\cap\cdots\cap\mathbf{R}_{\vec{\gamma}_{N-1}}} \xi_{N-1}(\mathbf{x})\,d\mathbf{x} + \cdots \\ &+ \int_{\mathbf{R}^c_{\vec{\gamma}_1}\cap\mathbf{R}^c_{\vec{\gamma}_2}\cap\mathbf{R}^c_{\vec{\gamma}_3}\cap\cdots\cap\mathbf{R}^c_{\vec{\gamma}_{N-1}}} \xi_N(\mathbf{x})\,d\mathbf{x} + \cdots \\ &+ \lambda\sum_{j=1}^{N-1}\oint_{\vec{\gamma}_j} ds. \end{aligned} \tag{4}$$

3.3. Curve evolution equations

The minimization of the functional E in Eq. (4) with respect to the curves $(\vec{\gamma}_j)_j$ is again performed by embedding the family $\vec{\gamma}_i : [0,1] \to \Omega,\ i = 1,\ldots,N-1$ of plane curves into a one-parameter family $\vec{\gamma}_i : [0,1]\times\mathbb{R}^+ \to \Omega$, $i = 1,\ldots,N-1$ of plane curves constructed by solving the following system of evolution equations:

$$\frac{d\vec{\gamma}_j}{dt} = -\frac{\delta E}{\delta\vec{\gamma}_j}, \quad j = 1,\ldots,N-1.$$

The functional derivatives $\frac{\delta E}{\delta\vec{\gamma}_j}$ can be easily computed by suitably rewriting the area integrals appearing in the energy functional. Starting with $\vec{\gamma}_1$, we can rewrite the energy functional Eq. (4) as follows:

$$\begin{aligned}E[\{\vec{\gamma}_i\}_{i=1}^{N-1}] = &\int_{\mathbf{R}_{\vec{\gamma}_1}} \xi_1(\mathbf{x})\,d\mathbf{x} + \int_{\mathbf{R}^c_{\vec{\gamma}_1}} \Phi_1(\mathbf{x})\,d\mathbf{x} + \lambda\oint_{\vec{\gamma}_1} ds \\ &+ \lambda\sum_{j=2}^{N-1}\oint_{\vec{\gamma}_j} ds, \end{aligned} \tag{5}$$

where $\Phi_1(\mathbf{x})$ is defined as

$$\begin{aligned}\Phi_1(\mathbf{x}) = &\xi_2(\mathbf{x})\chi_{\mathbf{R}_{\vec{\gamma}_2}}(\mathbf{x}) + \xi_3(\mathbf{x})\chi_{\mathbf{R}^c_{\vec{\gamma}_2}}(\mathbf{x})\chi_{\mathbf{R}_{\vec{\gamma}_3}}(\mathbf{x}) + \cdots \\ &+ \xi_{N-1}(\mathbf{x})\chi_{\mathbf{R}^c_{\vec{\gamma}_2}}(\mathbf{x})\chi_{\mathbf{R}^c_{\vec{\gamma}_3}}(\mathbf{x})\cdots\chi_{\mathbf{R}^c_{\vec{\gamma}_{N-2}}}(\mathbf{x})\chi_{\mathbf{R}_{\vec{\gamma}_{N-1}}}(\mathbf{x}) \\ &+ \xi_N(\mathbf{x})\chi_{\mathbf{R}^c_{\vec{\gamma}_2}}(\mathbf{x})\chi_{\mathbf{R}^c_{\vec{\gamma}_3}}(\mathbf{x})\cdots\chi_{\mathbf{R}^c_{\vec{\gamma}_{N-2}}}(\mathbf{x})\chi_{\mathbf{R}^c_{\vec{\gamma}_{N-1}}}(\mathbf{x}).\end{aligned}$$

Since $\Phi_1(\mathbf{x})$ and $\sum_{j=2}^{N-1}\oint_{\vec{\gamma}_j} ds$ have no dependence on $\vec{\gamma}_1$, the functional derivative $\frac{\delta E}{\delta\vec{\gamma}_1}$ is computed as for the standard region competition functional described in [17], yielding:

$$\frac{\delta E}{\delta\vec{\gamma}_1}(\vec{\gamma}_1(s,t)) = [\xi_1(\vec{\gamma}_1(s,t)) - \Phi_1(\vec{\gamma}_1(s,t)) + \lambda\kappa_1(s,t)]\vec{n}_1(s,t),$$

where $\vec{n}_1$ is the outward unit normal to $\vec{\gamma}_1$, and κ_1 the curvature function of $\vec{\gamma}_1$.

To compute the functional derivative $\frac{\delta E}{\delta\vec{\gamma}_2}$ yielding the evolution equation of $\vec{\gamma}_2$, we rewrite the energy functional Eq. (5) as follows:

$$\begin{aligned}E[\{\vec{\gamma}_i\}_{i=1}^{N-1}] = &\int_{\mathbf{R}_{\vec{\gamma}_1}} \xi_1(\mathbf{x})\,d\mathbf{x} + \int_{\mathbf{R}_{\vec{\gamma}_2}} \chi_{\mathbf{R}_1^c}(\mathbf{x})\xi_2(\mathbf{x})\,d\mathbf{x} \\ &+ \int_{\mathbf{R}^c_{\vec{\gamma}_2}} \chi_{\mathbf{R}_1^c}(\mathbf{x})\Phi_2(\mathbf{x})\,d\mathbf{x} + \lambda\oint_{\vec{\gamma}_2} ds \\ &+ \lambda\sum_{j\neq 2}\oint_{\vec{\gamma}_j} ds, \end{aligned} \tag{6}$$

where $\Phi_2(\mathbf{x})$ is defined as

$$\begin{aligned}\Phi_2(\mathbf{x}) = &\xi_3(\mathbf{x})\chi_{\mathbf{R}_{\vec{\gamma}_3}}(\mathbf{x}) + \xi_4(\mathbf{x})\chi_{\mathbf{R}^c_{\vec{\gamma}_3}}(\mathbf{x})\chi_{\mathbf{R}_{\vec{\gamma}_4}}(\mathbf{x}) + \cdots \\ &+ \xi_{N-1}(\mathbf{x})\chi_{\mathbf{R}^c_{\vec{\gamma}_3}}(\mathbf{x})\chi_{\mathbf{R}^c_{\vec{\gamma}_4}}(\mathbf{x})\cdots\chi_{\mathbf{R}^c_{\vec{\gamma}_{N-2}}}(\mathbf{x})\chi_{\mathbf{R}_{\vec{\gamma}_{N-1}}}(\mathbf{x}) \\ &+ \xi_N(\mathbf{x})\chi_{\mathbf{R}^c_{\vec{\gamma}_3}}(\mathbf{x})\chi_{\mathbf{R}^c_{\vec{\gamma}_4}}(\mathbf{x})\cdots\chi_{\mathbf{R}^c_{\vec{\gamma}_{N-2}}}(\mathbf{x})\chi_{\mathbf{R}^c_{\vec{\gamma}_{N-1}}}(\mathbf{x}).\end{aligned}$$

Here again, since $\int_{\mathbf{R}_{\vec{\gamma}_1}} \xi_1(\mathbf{x})\,d\mathbf{x}$, $\Phi_2(\mathbf{x})$, and $\sum_{j\neq 2}\oint_{\vec{\gamma}_j} ds$ have no dependence on $\vec{\gamma}_2$, the functional derivative of the first term in the right-hand side of Eq. (6) is null and the functional derivative $\frac{\delta E}{\delta\vec{\gamma}_2}$ is computed as for the standard region competition functional, yielding:

$$\begin{aligned}\frac{\delta E}{\delta\vec{\gamma}_2}(\vec{\gamma}_2(s,t)) = &\Big(\chi_{\mathbf{R}_1^c}(\vec{\gamma}_2(s,t))[\xi_2(\vec{\gamma}_2(s,t)) - \Phi_2(\vec{\gamma}_1(s,t))] \\ &+\lambda\kappa_2(s,t))\vec{n}_2(s,t),\end{aligned} \tag{7}$$

where $\vec{n}_2$ is the outward unit normal to $\vec{\gamma}_2$, and κ_2 the curvature function of $\vec{\gamma}_2$. This equation defines the evolution of $\vec{\gamma}_2$ outside the region $\mathbf{R}_1$, but says nothing about the evolution of the curve inside the region. Since the evolution of $\vec{\gamma}_2$ inside $\mathbf{R}_1$ does not affect the energy functional, we can define the evolution of $\vec{\gamma}_2$ inside the region $\mathbf{R}_1$ in the better way for the implementation. We have chose to simply extend to the whole curve the evolution strategy defined by Eq. (7). This will prove useful later while implementing the algorithm. The evolution equation for $\vec{\gamma}_2$ becomes:

$$\frac{\delta E}{\delta\vec{\gamma}_2}(\vec{\gamma}_2(s,t)) = (\xi_2(\vec{\gamma}_2(s,t)) - \Phi_2(\vec{\gamma}_1(s,t)) + \lambda\kappa_2(s,t))\vec{n}_2(s,t).$$

Proceeding similarly to compute the functional derivatives $\frac{\delta E}{\delta\vec{\gamma}_j}$ for all j, the minimization of the multiregion competition functional is achieved through the following system of coupled curve evolution equations:

$$\begin{cases} \frac{d\vec{\gamma}_1}{dt} &= -(\xi_1(\vec{\gamma}_1) - \Phi_1(\vec{\gamma}_1) + \lambda\kappa_1)\vec{n}_1, \\ \frac{d\vec{\gamma}_2}{dt} &= -(\xi_2(\vec{\gamma}_2) - \Phi_2(\vec{\gamma}_2) + \lambda\kappa_2)\vec{n}_2, \\ &\vdots \\ \frac{d\vec{\gamma}_j}{dt} &= -(\xi_2(\vec{\gamma}_j) - \Phi_j(\vec{\gamma}_j) + \lambda\kappa_j)\vec{n}_j, \\ &\vdots \\ \frac{d\vec{\gamma}_{N-1}}{dt} &= -(\xi_{N-1}(\vec{\gamma}_{N-1}) - \Phi_{N-1}(\vec{\gamma}_{N-1}) + \lambda\kappa_{N-1})\vec{n}_{N-1}, \end{cases} \tag{8}$$

where $\vec{n}_j$ is the outward unit normal to and κ_j the curvature function of $\vec{\gamma}_j$, for $j = 1, \ldots, N-1$, and $\Phi_j(\mathbf{x})$ is given by

$$\begin{aligned}\Phi_j(\mathbf{x}) = {} & \xi_{j+1}(\mathbf{x})\chi_{\mathbf{R}_{\vec{\gamma}_{j+1}}}(\mathbf{x}) + \xi_{j+2}(\mathbf{x})\chi_{\mathbf{R}^c_{\vec{\gamma}_{j+1}}}(\mathbf{x})\chi_{\mathbf{R}_{\vec{\gamma}_{j+2}}}(\mathbf{x}) + \cdots \\ & + \xi_{N-1}(\mathbf{x})\chi_{\mathbf{R}^c_{\vec{\gamma}_{j+1}}}(\mathbf{x})\cdots\chi_{\mathbf{R}^c_{\vec{\gamma}_{N-2}}}(\mathbf{x})\chi_{\mathbf{R}_{\vec{\gamma}_{N-1}}}(\mathbf{x}) \\ & + \xi_N(\mathbf{x})\chi_{\mathbf{R}^c_{\vec{\gamma}_{j+1}}}(\mathbf{x})\cdots\chi_{\mathbf{R}^c_{\vec{\gamma}_{N-2}}}(\mathbf{x})\chi_{\mathbf{R}^c_{\vec{\gamma}_{N-1}}}(\mathbf{x})\end{aligned}$$

for $j = 1, \ldots, N-1$.

3.4. Level set implementation

The system of Eq. (8) can be solved numerically by discretizing the interval $[0,1]$ on which the curves $(\vec{\gamma}_j)_{j=1}^{N-1}$ are defined, thus leading to a representation of $\vec{\gamma}_j$ $(j = 1, \ldots, N-1)$ in terms of a finite number of points or nodes. This leads to an *explicit* representation of $\vec{\gamma}_j$. A better alternative is to represent the curve $\vec{\gamma}_j$ *implicitly* by the zero level set of a function $u_j : \mathbb{R}^2 \to \mathbb{R}$ (with $j = 1, \ldots, N-1$), with the region inside $\vec{\gamma}_j$ corresponding to $u_j > 0$. There are well-known advantages to such an implicit representation [26], the most important being numerical stability and topology independence. There is also an additional advantage to using level set evolution equations in lieu of curve evolution equations, owing to the fact that region membership is explicitly maintained in the level set representation. Indeed, the sign of the function u_j determines which points are inside the curve $\vec{\gamma}_j$, and which points are outside it. This is of crucial importance in the context of our proposed multiregion competition functional, since as can be seen in the system of Eq. (8) numerous region indicator functions are involved, and bearing in mind that region membership is computationally very expensive to determine in the context of an explicit curve representation.

One can easily show [26] that if the evolution of $\vec{\gamma}_j$ is described by the equation

$$\frac{\mathrm{d}\vec{\gamma}_j(s,t)}{\mathrm{d}t} = F_j(\vec{\gamma}_j(s,t),t)\vec{n}_j(s,t),$$

where F_j is a real-valued function defined on $\mathbb{R}^2 \times \mathbb{R}^+$, then the corresponding evolution of u_j is given by:

$$\frac{\partial u_j(\mathbf{x},t)}{\partial t} = -F_j(\mathbf{x},t)\|\vec{\nabla}u_j(\mathbf{x},t)\|.$$

The level set evolution equations minimizing the functional (4) are therefore given by the following system of coupled partial differential equations:

$$\begin{cases} \frac{\partial u_1}{\partial t}(\mathbf{x},t) = (\xi_1(\mathbf{x}) - \Phi_1(\mathbf{x}) + \lambda\kappa_1)\|\vec{\nabla}u_1(\mathbf{x},t)\| \\ \qquad\vdots \\ \frac{\partial u_j}{\partial t}(\mathbf{x},t) = (\xi_j(\mathbf{x}) - \Phi_j(\mathbf{x}) + \lambda\kappa_j)\|\vec{\nabla}u_j(\mathbf{x},t)\| \\ \qquad\vdots \\ \frac{\partial u_{N-1}}{\partial t}(\mathbf{x},t) = (\xi_{N-1}(\mathbf{x}) - \Phi_{N-1}(\mathbf{x}) + \lambda\kappa_{N-1})\|\vec{\nabla}u_{N-1}(\mathbf{x},t)\|, \end{cases} \tag{9}$$

where $\Phi_j(\mathbf{x})$ is given by

$$\begin{aligned}\Phi_j(\mathbf{x}) = {} & \xi_{j+1}(\mathbf{x})\chi_{\{u_{j+1}(\mathbf{x},t)>0\}}(\mathbf{x}) \\ & + \xi_{j+2}(\mathbf{x})\chi_{\{u_{j+1}(\mathbf{x},t)\leqslant 0\}}(\mathbf{x})\chi_{\{u_{j+2}(\mathbf{x},t)>0\}}(\mathbf{x}) + \cdots \\ & + \xi_{N-1}(\mathbf{x})\chi_{\{u_{j+1}(\mathbf{x},t)\leqslant 0\}}(\mathbf{x})\cdots\chi_{\{u_{N-2}(\mathbf{x},t)\leqslant 0\}}(\mathbf{x})\chi_{\{u_{N-1}(\mathbf{x},t)>0\}}(\mathbf{x}) \\ & + \xi_N(\mathbf{x})\chi_{\{u_{j+1}(\mathbf{x},t)\leqslant 0\}}(\mathbf{x})\cdots\chi_{\{u_{N-2}(\mathbf{x},t)\leqslant 0\}}(\mathbf{x})\chi_{\{u_{N-1}(\mathbf{x},t)\leqslant 0\}}(\mathbf{x})\end{aligned}$$

with $\chi_{\{u_k(\mathbf{x},t)\leqslant 0\}} = 1$ if $u_k(\mathbf{x},t) \leqslant 0$ and 0 otherwise and κ_j being the curvature of the level set of u_j. The curvature κ is given as a function of u by the following expression:

$$\begin{aligned}\kappa = {} & \vec{\nabla}\cdot\frac{\vec{\nabla}u}{\|\vec{\nabla}u\|} \\ = {} & \frac{u_{xx}u_y^2 - 2u_xu_yu_{xy} + u_{yy}u_x^2}{(u_x^2+u_y^2)^{3/2}}.\end{aligned} \tag{10}$$

We should note that the equations in system Eq. (9) are only defined for points $(\mathbf{x},t)$ on the curves $\vec{\gamma}_j$. There is, however, an easy way to extend this evolution equations to the whole image domain. Given that the evolution of the function u_k for all points *not* in the zero levelset does not affect the energy, we can make these points evolve in the most convenient way for the implementation. We chose simply to use the same evolution equation for the whole image domain. This is possible because we have previously extended the evolution of curves $\vec{\gamma}_k$ to the whole image domain and is a characteristic of our algorithm that is not present in other algorithms.

Defining

$$\mathbf{R}_{u_i}(t) = \{\mathbf{x} \in \Omega | u_i(\mathbf{x},t) > 0\}, \quad i = 1, \ldots, N-1$$

the desired segmentation is then given by the family

$$\begin{aligned}&\{\mathbf{R}_{u_1}(t), \mathbf{R}_{u_1}(t)^c \cap \mathbf{R}_{u_2}(t), \\ &\mathbf{R}_{u_1}(t)^c \cap \mathbf{R}_{u_2}(t)^c \cap \mathbf{R}_{u_3}(t), \ldots, (\cup_{j=1}^{N-1}\mathbf{R}_{u_j}(t))^c\}\end{aligned}$$

as $t \to \infty$. The system Eq. (9) of level set evolution equations is solved by replacing time derivatives by finite differences, and spatial derivatives by approximations using forward and backward differences, as suggested in [26], the key idea of such numerical approximations being that the numerical domain of dependence of a function should contain its mathematical domain of dependence [26]. We refer the reader to [26] for a presentation and discussion of level set partial differential equation discretization schemes as well as for a presentation and analysis of algorithms for fast computation of level set evolution equations.

4. Motion/disparity-based segmentation

For motion/disparity segmentation we need to consider a sequence of images. Let $(\mathbf{I}_k)_k : \Omega \to \mathbb{R}^n$, $k = 1, \ldots, K$, be a sequence of image functions, with common domain $\Omega \subset \mathbb{R}^2$. For motion- or stereo-based image segmentation, $(\mathbf{I}_k)_k$ contains two images (two images taken at consecutive

instants of time in the case of motion, and a pair of stereoscopic images in the case of disparity).

The Bayesian formulation of the segmentation problem becomes:

$$\{\hat{\mathbf{R}}_i\}_{i=1}^{N} = \arg\max_{\{\mathbf{R}_i \subset \Omega\}} P((\mathbf{I}_k)_k|\{\mathbf{R}_i\})P(\{\mathbf{R}_i\}),$$

where $P((\mathbf{I}_k)_k|\{\mathbf{R}_i\})$ is the likelihood of the segmentation, and $P(\{\mathbf{R}_i\})$ its prior. For motion, and stereo-based segmentation, image formation can be modeled by:

$$\mathbf{I}_l = \sum_{j=1}^{N}((\mathbf{I}_{l+1} \circ T_j) + \mu_j)\chi_{\mathbf{R}_j} \tag{11}$$

with $T_j : \Omega \to \Omega$ the motion (resp. stereo) transformation corresponding to region $\mathbf{R}_j$, i.e., two consecutive images of the sequence differ in the placement of their moving regions. Model Eq. (11) is common in motion (disparity) segmentation [39].

We will assume, as in Section 2.1, that the T_j are independent of the segmentation $\{\mathbf{R}_i\}$ and that they are either computed prior to the segmentation or computed iteratively in parallel with the segmentation.

It is important to note that for motion and stereo segmentation, the image formation model given in Eq. (11) does not account for occluded regions. Such regions are negligible whenever the displacement or disparity is small, but become important for large displacements and disparities and must somehow be incorporated in the image formation model. In Section 5, we present an extension of the model Eq. (11) that takes into account deviations from this model.

With this model, and following a similar path as the one taken in Section 2.1, we obtain the expression of the energy to minimize:

$$E[\{\mathbf{R}_i\}_{i=1}^{N}] = \sum_{j=1}^{N} \int_{\mathbf{R}_j} \xi_j(\mathbf{x})\,d\mathbf{x} - \log P(\{\mathbf{R}_i\}) \tag{12}$$

with the function ξ_j redefined to reflect the new image formation model:

$$\xi_j(\mathbf{x}) \equiv \tfrac{1}{2}\log|\Sigma_j| + \tfrac{1}{2}(\mathbf{I}_l(\mathbf{x}) - (\mathbf{I}_{l+1} \circ T_j)(\mathbf{x}))^T \Sigma_j^{-1}(\mathbf{I}_l(\mathbf{x}) - (\mathbf{I}_{l+1} \circ T_j)(\mathbf{x})). \tag{13}$$

The curve evolution algorithm developed in Section 3 can, therefore, be applied to solve this minimization problem.

5. Extended image formation model

The basic image formation model presented in the previous Section is accurate insofar as the image function $\mathbf{I}_l$ can be expressed, up to an additive noise term, as the linear combination given in Eq. (11). As was mentioned in Section 4, there are numerous cases where an image formation model such as in Eq. (11) does not capture the complexity of the observed image: this is the case for large range motion, which leaves large portions of the image occluded and hence unexplainable by any reasonable geometric transformation, as well as for large disparity stereo, which leads to numerous portions of one image which have no correspondence in the other. We shall refer to image points which cannot be explained by the image formation model Eq. (11) as *outliers*. The multiregion competition algorithm presented in Section 3 leads to an image partition which does not account for outliers. As a result, outliers are distributed among the N regions of the partition, with each outlier roughly assigned to the region which models it best. It is often desirable to explicitly account for the outliers and clearly discriminate them from the rest of the image points. To do so, we assume the image domain Ω is

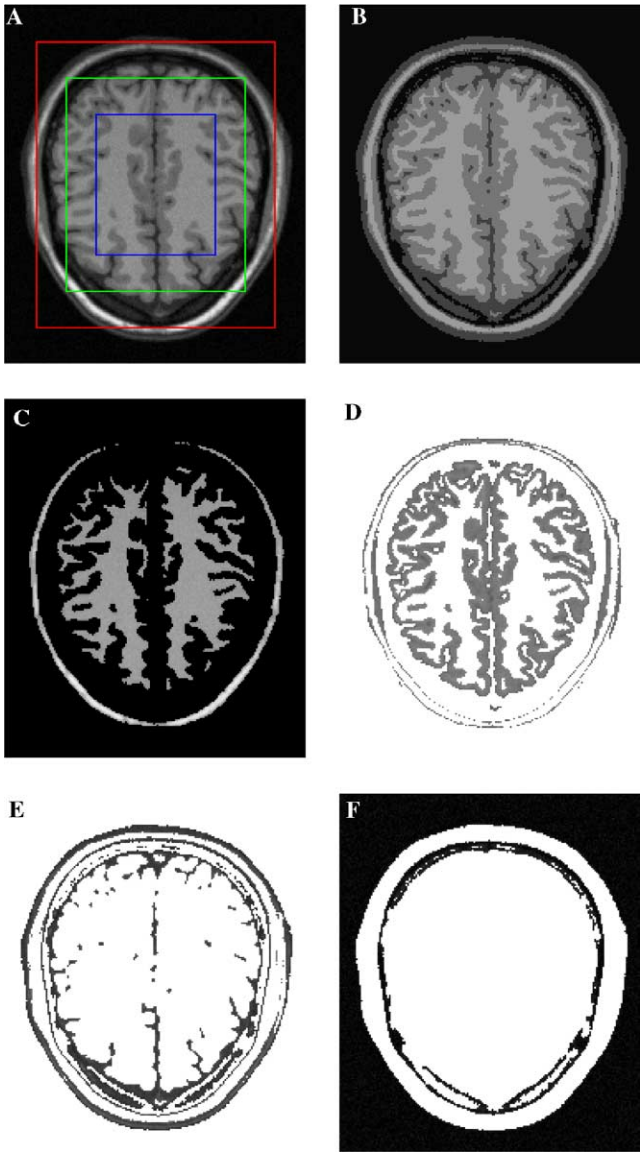

Fig. 2. Gray-level image segmentation. (A) Original image with initialization; (B) final segmentation represented by region's means; four segmented regions; (C) white matter; (D) gray matter; (E) dark zones; and (F) black background.

partitioned into a family $\{\mathbf{R}_i\}_{i=1}^{N+1}$ of $N+1$ regions, with region $\mathbf{R}_{N+1}$ corresponding to the subset of outliers of the image. The corresponding image formation model is then given by

$$\mathbf{I}_l = \begin{cases} \sum_{j=1}^{N+1} (\mathbf{I}_{l+1} \circ T_j)\chi_{\mathbf{R}_j} + \mu & \text{on} \quad \bigcup_{j=1}^{N} \mathbf{R}_j, \\ v & \text{on} \quad \mathbf{R}_{N+1}, \end{cases} \tag{14}$$

where v is an independent stationary random process uniformly distributed at each point. Performing the same steps as in Section 3, the Bayesian estimator of the segmentation $\{\mathbf{R}_i\}_{i=1}^{N+1}$ is given by the following energy minimization problem:

$$\{\hat{\mathbf{R}}_i\}_{i=1}^{N} = \arg \min_{\{\mathbf{R}_i \subset \Omega\}} E[\{\mathbf{R}_i\}_{i=1}^{N+1}],$$

where the energy $E[\{\mathbf{R}_i\}_{i=1}^{N+1}]$ is defined by

$$E[\{\mathbf{R}_i\}_{i=1}^{N+1}] = \frac{1}{2\sigma^2} \sum_{j=1}^{N} \int_{\mathbf{R}_j} (\mathbf{I}_l(\mathbf{x}) - (\mathbf{I}_{l+1} \circ T_j)(\mathbf{x}))^2 \, d\mathbf{x} + \int_{\mathbf{R}_{N+1}} C \, d\mathbf{x} - \log P(\{\mathbf{R}_i\}), \tag{15}$$

where C is a constant. As in Section 3, the minimization of this functional is done by first considering a family of plane curves; however, given that $N+1$ regions need now to be

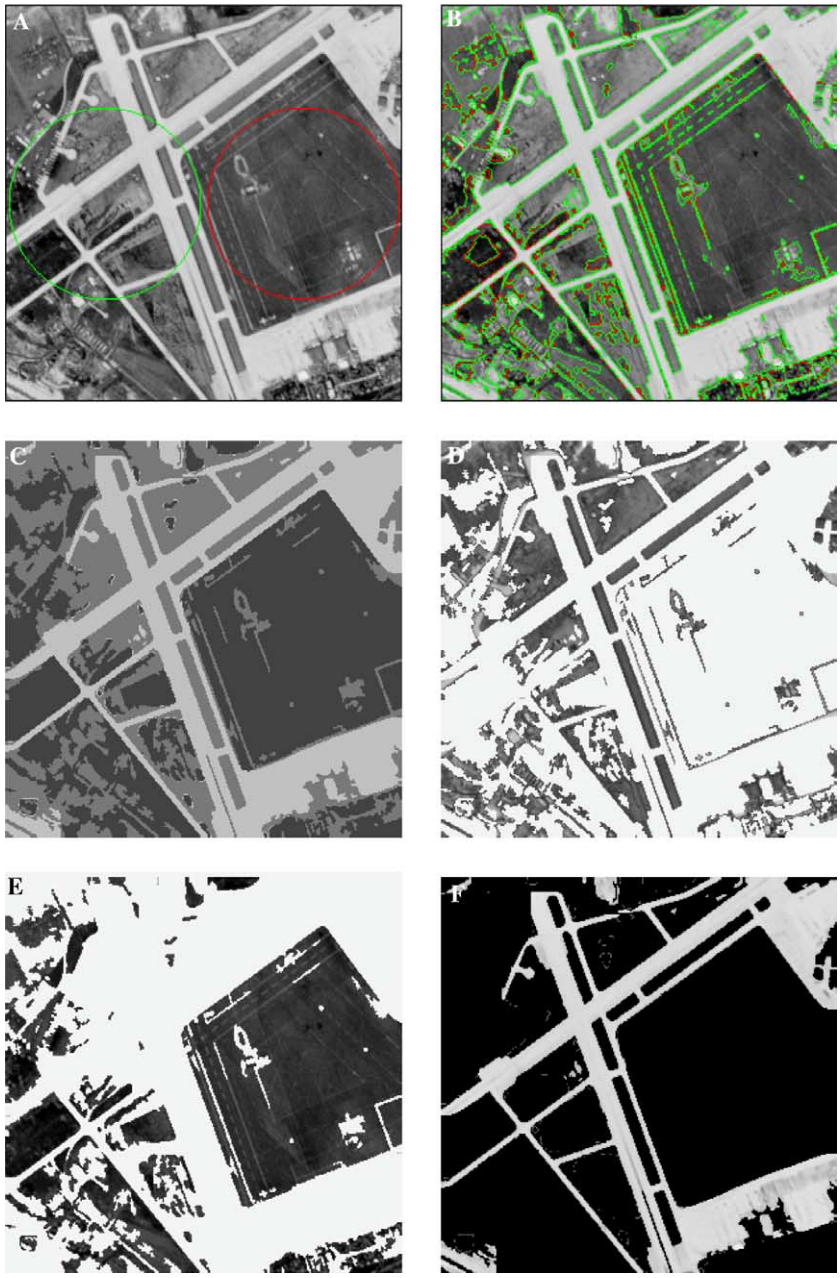

Fig. 3. Gray-level image segmentation. (A) Original image with initialization; (B) algorithm evolution; (C) final segmentation represented by region's means; three segmented regions; (D) green spaces; (E) paved zones and; (F) airport driveway.

estimated, a family $(\vec{\gamma}_j)_{j=1}^N$ of N plane curves is defined (as opposed to $N-1$ in Section 3). In a manner similar to that in Section 3, the correspondence between the family of plane curves $(\vec{\gamma}_j)_{j=1}^N$ and the image segmentation is established by assigning the region $\mathbf{R}_{\vec{\gamma}_1}$ inside the curve $\vec{\gamma}_1$ to region $\mathbf{R}_1$ of the segmentation, the region $\mathbf{R}^c_{\vec{\gamma}_1} \cap \mathbf{R}_{\vec{\gamma}_2}$ to region $\mathbf{R}_2$ of the segmentation, the region $\mathbf{R}^c_{\vec{\gamma}_1} \cap \mathbf{R}^c_{\vec{\gamma}_2} \cap \mathbf{R}_{\vec{\gamma}_3}$ to region $\mathbf{R}_3$ of the segmentation, ..., the region $\mathbf{R}^c_{\vec{\gamma}_1} \cap \mathbf{R}^c_{\vec{\gamma}_2} \cap \cdots \cap \mathbf{R}^c_{\vec{\gamma}_{N-1}} \cap \mathbf{R}_{\vec{\gamma}_N}$ to region $\mathbf{R}_N$ of the segmentation, and finally the region $\mathbf{R}^c_{\vec{\gamma}_1} \cap \mathbf{R}^c_{\vec{\gamma}_2} \cap \cdots \cap \mathbf{R}^c_{\vec{\gamma}_{N-1}} \cap \mathbf{R}^c_{\vec{\gamma}_N}$ to region $\mathbf{R}_{N+1}$ of the segmentation, that is, the region consisting of outliers. The energy functional to minimize as a function of the curves $\{\vec{\gamma}_i\}$ is thus given by:

$$E[(\vec{\gamma}_i)_{i=1}^{N-1}] = \frac{1}{2\sigma^2}\left\{\sum_{j=1}^{N}\int_{\mathbf{R}_{\vec{\gamma}_j}} \left(\mathbf{I}_l(\mathbf{x}) - \left(\mathbf{I}_{l+1}\circ T_j\right)(\mathbf{x})\right)^2 \mathrm{d}\mathbf{x}\right\} + \int_{(\cup_{j=1}^N \mathbf{R}_{\vec{\gamma}_j})^c} C\,\mathrm{d}\mathbf{x} - \log P(\{\vec{\gamma}_i\}).$$

The corresponding curve evolution equations are given by the system of equations

$$\left\{\frac{\mathrm{d}\vec{\gamma}_j}{\mathrm{d}t} = -\left(\xi_j(\vec{\gamma}_j) - \Phi_j(\vec{\gamma}_j) + \lambda\kappa_j\right)\vec{n}_j, \qquad j = 1,\ldots,N, \quad (16)$$

where $\Phi_j(\mathbf{x})$ is given for $j = 1,\ldots,N$ by

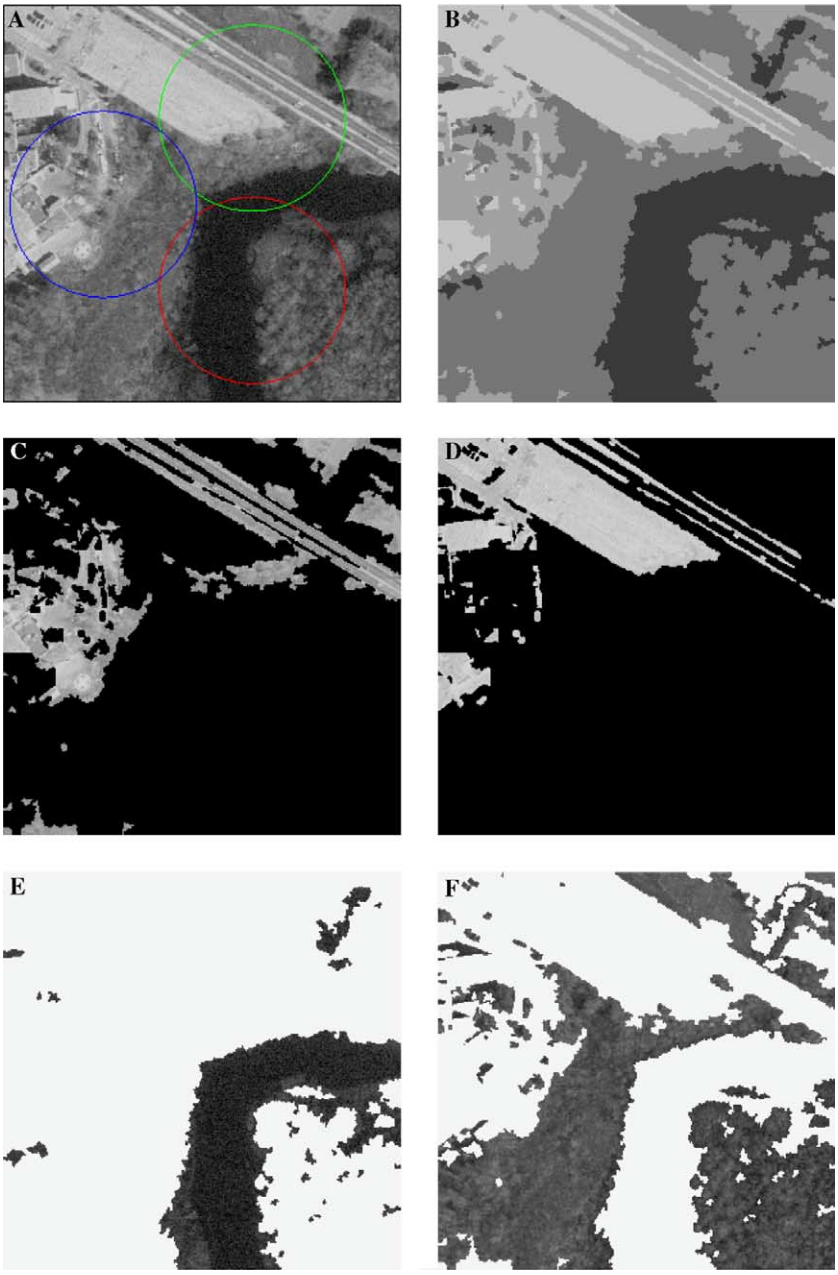

Fig. 4. Gray-level image segmentation. (A) Original image with initialization; (B) final segmentation represented by region's means; four segmented regions; (C) green spaces and highway; (D) parking lot and building roofs; (E) river and; (F) wood.

$$\begin{aligned}\Phi_j(\mathbf{x}) = {} & \xi_{j+1}(\mathbf{x})\chi_{\mathbf{R}_{\vec{\gamma}_{j+1}}}(\mathbf{x}) \\ & + \xi_{j+2}(\mathbf{x})\chi_{\mathbf{R}^c_{\vec{\gamma}_{j+1}}}(\mathbf{x})\chi_{\mathbf{R}_{\vec{\gamma}_{j+2}}}(\mathbf{x}) + \cdots \\ & + \xi_{N-1}(\mathbf{x})\chi_{\mathbf{R}^c_{\vec{\gamma}_{j+1}}}(\mathbf{x})\cdots\chi_{\mathbf{R}_{\vec{\gamma}_{N-1}}}(\mathbf{x})(\mathbf{x}) \\ & + \xi_N(\mathbf{x})\chi_{\mathbf{R}^c_{\vec{\gamma}_{j+1}}}(\mathbf{x})\cdots\chi_{\mathbf{R}^c_{\vec{\gamma}_{N-1}}}(\mathbf{x})\chi_{\mathbf{R}_{\vec{\gamma}_N}}(\mathbf{x}) \\ & + C\chi_{\mathbf{R}^c_{\vec{\gamma}_{j+1}}}(\mathbf{x})\cdots\chi_{\mathbf{R}^c_{\vec{\gamma}_{N-1}}}(\mathbf{x})\chi_{\mathbf{R}^c_{\vec{\gamma}_N}}(\mathbf{x})\end{aligned}$$

for $j = 1, \ldots, N$. The corresponding level set evolution equations are then given by the system:

$$\left\{\frac{\partial u_j}{\partial t}(\mathbf{x}, t) = -(\xi_j(\mathbf{x}) - \Phi_j(\mathbf{x}) + \lambda\kappa_j)\|\vec{\nabla}u_j(\mathbf{x}, t)\|, \right. \tag{17}$$

$(j = 1, \ldots, N)$ where $\Phi_j(\mathbf{x})$ is given by

$$\begin{aligned}\Phi_j(\mathbf{x}) = {} & \xi_{j+1}(\mathbf{x})\chi_{\{u_{j+1}(\mathbf{x},t)>0\}}(\mathbf{x}) \\ & + \xi_{j+2}(\mathbf{x})\chi_{\{u_{j+1}(\mathbf{x},t)\leqslant 0\}}(\mathbf{x})\chi_{\{u_{j+2}(\mathbf{x},t)>0\}}(\mathbf{x}) + \cdots \\ & + \xi_{N-1}(\mathbf{x})\chi_{\{u_{j+1}(\mathbf{x},t)\leqslant 0\}}(\mathbf{x})\cdots\chi_{\{u_{N-2}(\mathbf{x},t)\leqslant 0\}}(\mathbf{x})\chi_{\{u_{N-1}(\mathbf{x},t)>0\}}(\mathbf{x}) \\ & + \xi_N(\mathbf{x})\chi_{\{u_{j+1}(\mathbf{x},t)\leqslant 0\}}(\mathbf{x})\cdots\chi_{\{u_{N-1}(\mathbf{x},t)\leqslant 0\}}(\mathbf{x})\chi_{\{u_N(\mathbf{x},t)>0\}}(\mathbf{x}) \\ & + C\chi_{\{u_{j+1}(\mathbf{x},t)\leqslant 0\}}(\mathbf{x})\cdots\chi_{\{u_{N-1}(\mathbf{x},t)\leqslant 0\}}(\mathbf{x})\chi_{\{u_N(\mathbf{x},t)\leqslant 0\}}(\mathbf{x}).\end{aligned}$$

6. Experimental results

We ran several experiments to validate the formulation and its implementation. We show results of some of these experiments. These include segmentation of gray-scale images, color images, and motion-based segmentation.

In the experiments on gray scale and color images, we used the image model of Eq. (1). The parameter α_j has been taken to be the mean (gray scale or color) in region j. We estimate the mean vector α_j and covariance matrix Σ_j from image $\mathbf{I}$ by:

$$\begin{aligned}\alpha_j &= \left[\frac{\int_{\mathbf{R}_j}\mathbf{I}^{(h)}(\mathbf{x})\,d\mathbf{x}}{\int_{\mathbf{R}_j}d\mathbf{x}}\right] \\ \Sigma_j &= \left[\frac{\int_{\mathbf{R}_j}\mathbf{I}^{(h)}(\mathbf{x})\mathbf{I}^{(m)}(\mathbf{x})\,d\mathbf{x}}{\int_{\mathbf{R}_j}d\mathbf{x}} - \alpha_j^{(h)}\alpha_j^{(m)}\right],\end{aligned} \tag{18}$$

where $(h, m) \in [1, n]$.

In the experiments on motion-based segmentation we used the image models of Eqs. (11) and (14).

6.1. Segmentation of gray scale images

Fig. 2A shows a real image from an MRI brain scan. The original position of the level set contours are superimposed on the image. The computed segmentation, with regions represented by their means, is presented in Fig. 2B. In Figs. 2C–F, the four segmented regions on a contrasting background are shown.

Next, we show two examples of segmentation of aerial images. In Fig. 3, we show the image of an airport. Three regions can be identified in this image: the airport driveway, the paved zones and the green spaces. The computed segmentation is shown in Fig. 3C with regions represented by their means, and the three regions are shown on a contrasting background in Figs. 3D–F.

In Fig. 4, we show results for an urban scene. Fig. 4A, shows the original image along with the initialization. In this image there are four distinctive regions: the river and other water surfaces; the parking and building roofs; the wood; and the highway and green areas. The computed segmentation is shown in Fig. 4B with regions represented by their means, and the four segmented regions on a contrasting background are shown in Figs. 4C–F.

In all these examples the parameters of the regions (mean and covariance matrix) has been estimated progressively with the algorithm, thus no a priori information on the statistical characteristics of the regions has been used in the segmentation process. The computed segmentation

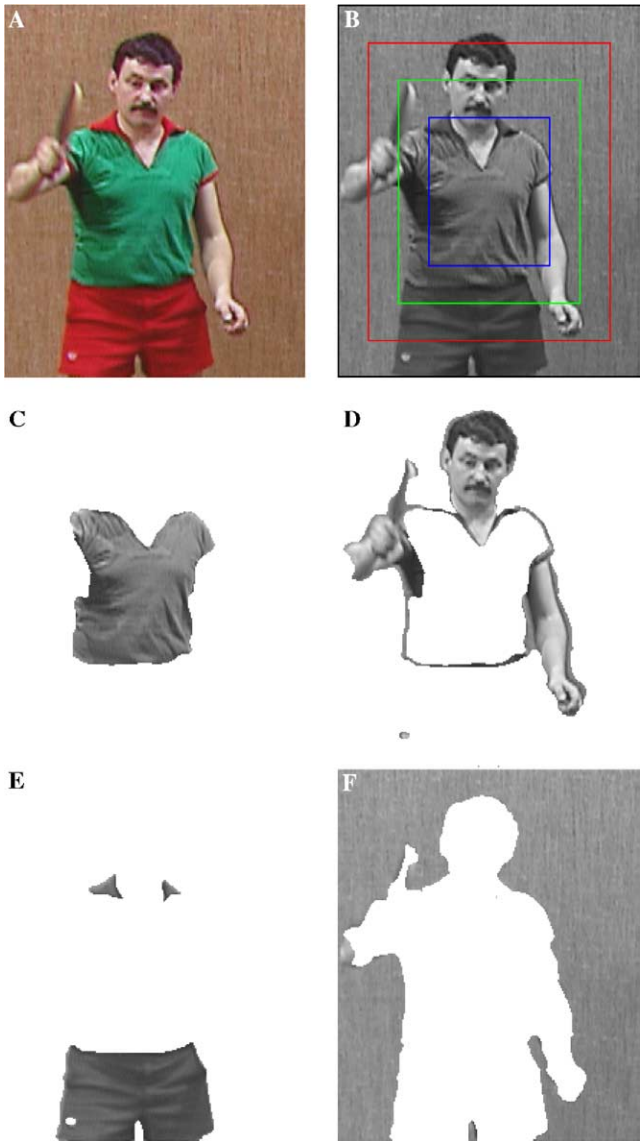

Fig. 5. Color image segmentation. (A) Original color image; (B) luminance image with initialization; four segmented regions; (C) shirt; (D) man and racket; (E) shorts and; (F) wall.

is very good and in conformity with expectations from visual inspection of the images.

6.2. Segmentation of color images

Many color spaces can be used to describe the color information in images, the more common being the RGB, YCMK, and YCbCr spaces. These spaces, however, are not perceptually uniform, making them a bad choice for color image segmentation. More uniform spaces from the point of view of color perception by the viewer have been developed. In our experiments, we use the CIElab color space [40, chapter 7]. The images used have been converted from their original color space to CIElab and the vector composed by the chrominance components (a,b) has been used as input to our algorithm. The luminance information has not been included.

We show the segmentation results for the image "Ping-pong," extracted from the homonymous video sequence which is a YCbCr 4:2:2 interlaced sequence. The color components have been then interpolated horizontal and vertically to match the size of the luminance image which is used as a reference to represent the evolution of the algorithm. The original color image is shown in Fig. 5A. The initial level set contours are shown in Fig. 5B superimposed on the luminance image. The final four segmented regions are presented in Figs. 5C–F. The segmentation is very good. The shirt, shorts, and wall regions has been almost perfectly segmented. The region corresponding to the man and the racket includes some bordering regions between the shirt and the wall or shorts. This is due to the interpolation process that smoothes the edges between regions, facilitating the capture of a thin border band by another region, in this case the man.

6.3. Motion-based segmentation

The purpose with this last example is twofold: to show the applicability of the algorithm to motion-based segmentation, and to demonstrate the extension of the algorithm on images with severe occlusions. The test images are natural images with synthetic long-range motion. As was noted in Section 2.1, long-range motion induces non-negligible zones of occlusion and provides a good testing ground for comparing the segmentation results derived from the basic model (corresponding to the system of coupled level set Eq. (9))

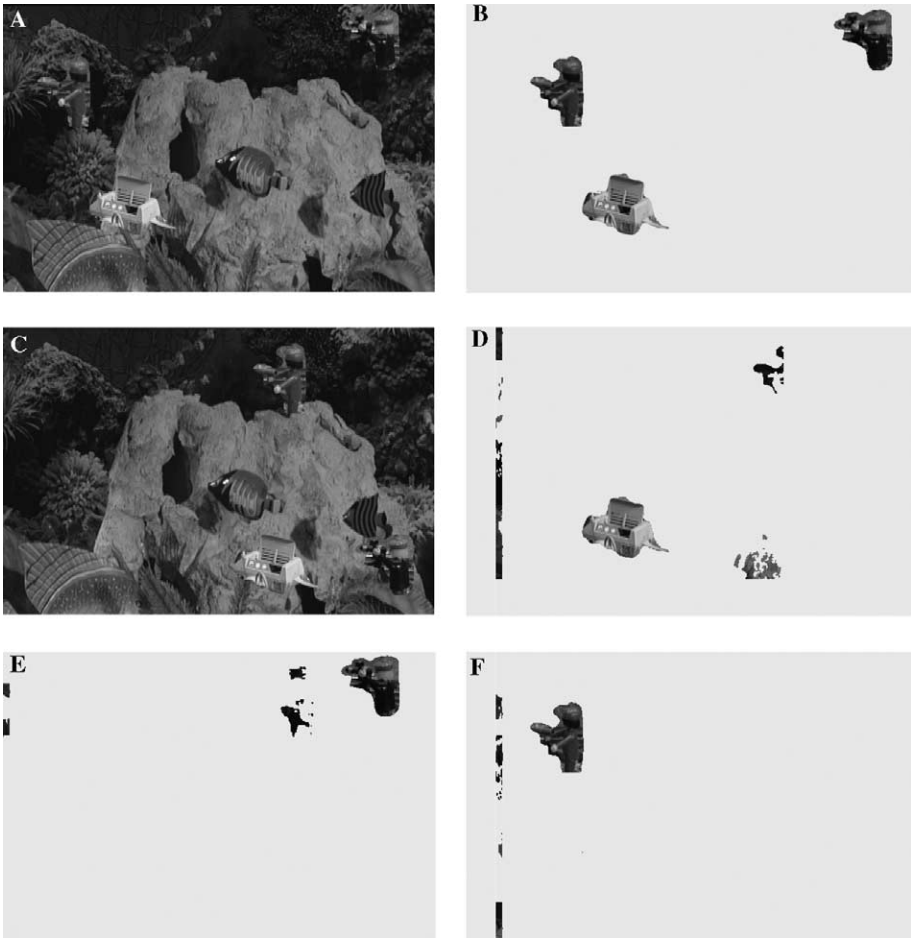

Fig. 6. Motion segmentation with the multiregion competition algorithm. (A) Image at time t ($\mathbf{I}_0$); (B) moving regions (excluding background) in $\mathbf{I}_0$; (C) image at time $t+1$ ($\mathbf{I}_1$); Segmentation results obtained by level set evolution according to the system Eq. (9); (D) generator; (E) cameraman; (F) figurine.

and those derived from the extended model (corresponding to the system of coupled level set Eq. (17)).

Fig. 6A is constructed by pasting onto the first frame of the (left) *aqua* stereoscopic sequence cutouts extracted from the first frame of the (left) *tunnel* stereoscopic sequence. There are three such cutouts: the generator, to the lower left of Fig. 6A, the little figurine, to the upper left of Fig. 6A, and the little cameraman figurine in the upper-right portion of Fig. 6A. Fig. 6B shows these three cutouts on a plain background. Fig. 6C shows the result of inducing translational motion on the three cutouts as well as on the background of Fig. 6A: the figurine to the left has moved slightly up and to the right, the cameraman figurine to the right has moved slightly right and down, the generator has moved down and right, and the background has moved left. The goal of motion segmentation is to recover the individual cutouts depicted in Fig. 6B from the images in Fig. 6A ($\mathbf{I}_0$) and (C) ($\mathbf{I}_1$). As mentioned in Section 2.1, we assume the translation parameters of each of the four regions to be known prior to the segmentation: We describe in detail in [21] how motion parameters can be recovered prior to, and independently of, any motion segmentation. Figs. 6D–F and Fig. 7A show the results of motion-based segmentation via the multiregion competition algorithm given by level set evolution Eq. (9) for the generator, cameraman, figurine, and background, respectively. As can be seen in all four images, the individual regions have been precisely recovered; however, due to the fact that the evolution Eq. (9) provide no outliers rejection mechanism, substantial portions of the occluded regions have been assigned to the four motion regions. This problem is considerably reduced by considering the system of level set evolution Eq. (17) corresponding to multiregion competition *with* outliers rejection. The results of this segmentation are shown in Figs. 7B–E for the generator, cameraman, figurine, and background, respectively. As can be seen in all four images, the individual motion regions have been precisely segmented as before; this time however, far fewer outliers have been assigned to the motion regions. In Fig. 7D, no outliers has been assigned to the motion region of the figurine, while in Figs. 7B and 7C some outliers have been assigned to the motion regions corresponding to the generator and the cameraman, respectively. This is due to the fact that those outliers have been accidentally well

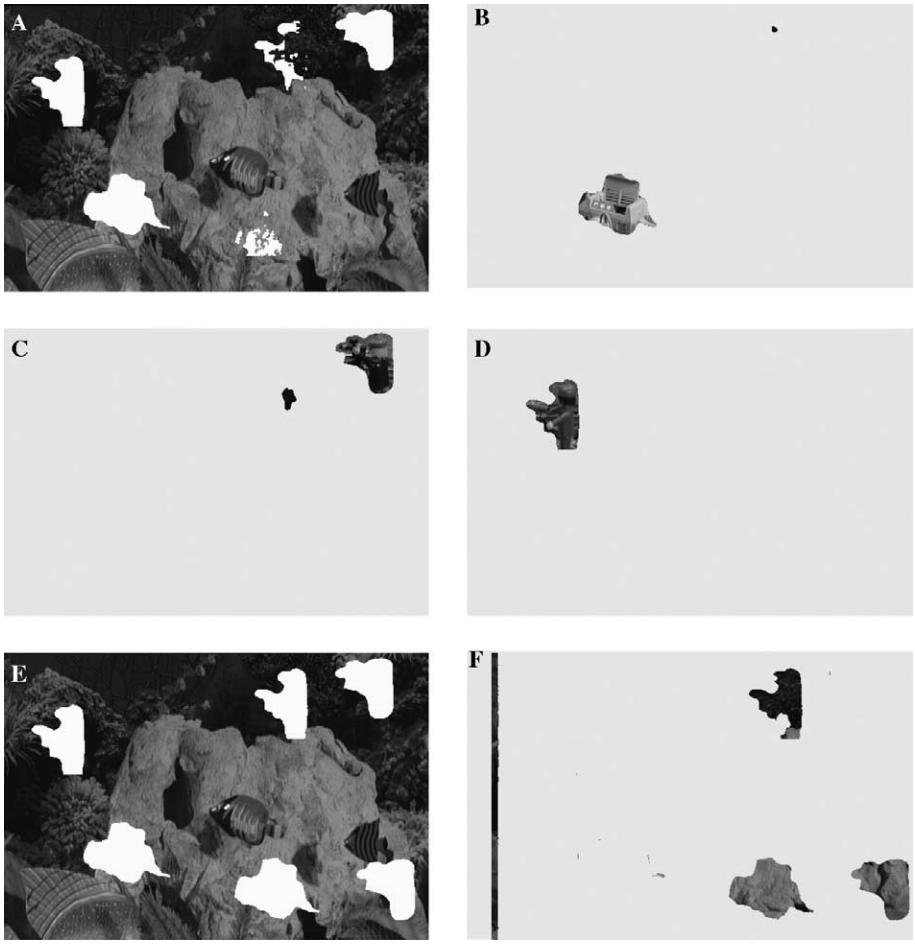

Fig. 7. Motion segmentation with the multiregion competition algorithm. (A) Segmentation of the background obtained by level set evolution according to the system Eq. (9). Segmentation results obtained by level set evolution according to the system Eq. (17); (B) generator; (C) cameraman; (D) figurine; (E) background; (F) occlusion regions.

explained (in the sense of low motion residual) by the motion transformations of the regions to which they have been assigned. Decreasing the value of the constant C reduces such regions, while increasing C increases these regions. Fig. 7E shows the segmented background region: it is important to note here that both the motion regions and the regions they occlude have been excluded from the background, as should be the case, and in sharp contrast to the background segmentation obtained in Fig. 7A. Fig. 6F shows the occluded regions obtained by the multiregion competition algorithm: There are four such regions, the three shapes to the right corresponding to the occlusion regions of the three cutouts, and the vertical strip to the left corresponding to the occlusion region of the background (recall the background is moving leftwards).

7. Conclusion

We have presented a level set multiregion competition algorithm, a natural level set extension to multiple regions of the well-known region competition algorithm. Our proposed algorithm reduces to the standard region competition algorithm whenever only two regions are considered. Its main feature is that the resulting segmentation, into a fixed but arbitrary number of regions, is guaranteed to be a partition of the image domain. This ensures that no ambiguities arise when assigning points to the various segmented regions. Our starting point was a Bayesian formulation of the segmentation problem, leading to curve evolution equations which are then formulated as level set partial differential equations. We have presented an extension of the multiregion competition algorithm which accounts for modeling inaccuracies and imperfections, leading to an outliers rejection mechanism. The experimental results we have shown clearly illustrate the fact that the final segmentation remains a partition of the image domain; they also clearly highlight the difference in segmentation that is obtained with and without the extension for outliers rejection.

Acknowledgment

This research was supported in part by the Natural Sciences and Engineering Research Council of Canada under strategic Grant STR224122.

References

[1] C. Papin, P. Bouthemy, P. Perez, Unsupervized segmentation of low clouds from infrared METEOSTAT images based on a contextual spatio-temporal labeling approach, IEEE Trans. Geosci. Remote Sensing 40 (1) (2002) 104–114.
[2] D.L. Pham, C. Xu, J. Prince, Current methods in medical image segmentation, Ann Rev. Biomed. Eng. 2 (1) (2000) 315–338.
[3] J. Odobez, P. Bouthemy, Direct model-based image segmentation for dynamic scene analysis, in: S.Z. Li et al. (Eds.), Recent Developments in Computer Vision, Springer Verlag, Berlin, 1996, pp. 91–100.
[4] Q. Cai, J. Aggarwal, Human motion analysis: A review, Comput. Vis. Image Understand. 73 (3) (1999) 428–440.
[5] E. Sifakis, G. Tziritas, Moving object localization using a multi-label fast marching algorithm, Signal Process.: Image Commun. 16 (2001) 963–976.
[6] I. Celasun, A. Tekalp, M. Gokcetekin, D. Harmanci, 2-D mesh-based video object segmentation and tracking with occlusion resolution, Signal Process.: Image Commun. 16 (2001) 950–962.
[7] F. Idriss, S. Panchanathan, Review of image and video indexing techniques, J. Vis. Commun. Image Represent. 8 (2) (1997) 146–166.
[8] M. Kass, A. Witkin, D. Terzopoulos, Snakes: active contour models, Inter. J. Comput. Vis. 1 (1987) 321–331.
[9] D. Terzopoulos, A. Witkin, Constraints on deformable models: recovering shape and non-rigid motion, Artif. Intell. 36 (1988) 91–123.
[10] A. Blake, A. Yuille, Active Vision, MIT Press, Cambridge, MA, 1992.
[11] V. Caselles, F. Catte, T. Coll, F. Dibos, A geometric model for active contours in image-processing, Numer. Math. 66 (11) (1993) 1–31.
[12] D. Mumford, J. Shah, Optimal approximations by piecewise smooth functions and associated variational-problems, CPAM 42 (5) (1989) 577–685.
[13] L. Cohen, On active contour models and balloons, CVGIP: Image Understand. 53 (1991) 211–218.
[14] V. Caselles, R. Kimmel, G. Sapiro, Geodesic active contours, Intern. J. Comput. Vis. 22 (1) (1997) 61–79.
[15] S. Kichenassamy, A. Kumar, P. Olver, A. Tannenbaum, A. Yezzi, Conformal curvature flows: from phase transitions to active vision, ARMA 134 (3) (1996) 275–301.
[16] R. Fonfard, Region-based strategies for active contour models, Intern. J. Comput. Vis. 13 (2) (1994) 229–251.
[17] S. Zhu, A. Yuille, Region competition: unifiying snakes, region growing, and bayes/MDL for multiband image segmentation, IEEE Trans. Pattern Anal. Mach. Intell. 18 (9) (1996) 884–900.
[18] C. Samson, L. Blanc-Féraud, G. Aubert, J. Zerubia, A level set method for image classification, in: Proc. Inter. Conf. Scale-Space Theories in Computer Vision, Corfu, Greece, 1999, pp. 306–317.
[19] T. Chan, B. Sandberg, L. Vese, Active contours without edges for vector-valued images, J. Vis. Commun. Image Represent. 11 (2) (2000) 130–141.
[20] L. Vese, T. Chan, A multiphase level set framework for image segmentation using the Mumford and Shah model, Intern. J. Comput. Vis. 50 (3) (2002) 271–293.
[21] A.-R. Mansouri, J. Konrad, Multiple motion segmentation with level sets, in: Proc. IEEE Inter. Conf. Image Processing, vol. II, 1999, pp. 126–130.
[22] N. Paragios, R. Deriche, Coupled geodesic active regions for image segmentation: a level set approach, in: Proc. Eur. Conf. Computer Vision, Dublin, Ireland, 2000, pp. 224–240.
[23] M. Rousson, R. Deriche, A variational framework for active and adaptative segmentation of vector valued images, in: Proc. IEEE Workshop on Motion and Video Computing, Orlando, FL, 2002, pp. 56–61.
[24] A. Yezzi, A. Tsai, A. Willsky, A fully global approach to image segmentation via coupled curve evolution equations, J. Vis. Commun. Image Represent. 13 (1) (2002) 195–216.
[25] S. Osher, J. Sethian, Front propagation with curvature dependent speed: algorithms based on Hamilton–Jacobi formulations, J. Comput. Phys. 79 (1988) 12–49.
[26] J. Sethian, Level Set Methods and Fast Marching Methods, Cambridge University Press, 1999.
[27] K. Smith, F. Solis, D. Chopp, A projection method for motion of triple junctions by level sets, Interfaces Free Boundaries 4 (3) (2002) 263–276.
[28] A. Mitiche, R. Feghali, A. Mansouri, Motion tracking as spatio-temporal motion boundary detection, J. Robot. Auton. Syst. 43 (2003) 39–50.
[29] A.-R. Mansouri, A. Mitiche, R. Feghali, Spatio-temporal motion segmentation via level sets partial differential equations, in: Proc. IEEE Southwest Symposium on Image Analysis and Interpretation, Santa Fe, NM, USA, 2002, pp. 243–247.

[30] A.-R. Mansouri, A. Mitiche, Spatial/joint space-time motion segmentation of images sequences by level set pursuit, in: Proc. IEEE Inter. Conf. Image Processing, vol. II, Rochester, NY, USA, 2002, pp. 265–268.
[31] A.-R. Mansouri, A. Mitiche, Region tracking via local statistics and level set PDEs, in: Proc. IEEE Inter. Conf. Image Processing, vol. III, Rochester, NY, USA, 2002, pp. 605–608.
[32] D. Cremers, S. Soatto, Variational space-time motion segmentation, in: Proc. IEEE Inter. Conf. Computer Vision, Nice, France, 2003, pp. 886–892.
[33] S. Jehan-Besson, M. Barlaud, G. Aubert, Detection and tracking of moving objects using a new level set based method, in: Proc. Inter. Conf. on Pattern Recognition, Barcelona, Spain, 2000, pp. 7112–7117.
[34] N. Paragios, R. Deriche, Geodesic active contours and level sets for the detection and tracking of moving objects, IEEE Trans. Pattern Anal. Mach. Intell. 22 (3) (2000) 266–280.
[35] A.-R. Mansouri, Region tracking via level set PDEs without motion computation, IEEE Trans. Pattern Anal. Mach. Intell. 24 (7) (2002) 947–961.
[36] B. Sandberg, T. Chan, L. Vese, A level-set and gabor-based active contour algorithm for segmenting textured images, Tech. Rep. CAM Report 02-39, University of California, UCLA, Los Angeles, CA, USA (Jul. 2002).
[37] S. Zhu, Y. Wu, D. Mumford, Filters, random fields, and minimax entropy (frame): toward a unified theory for texture modeling, in: Proc. Conf. on Comp. Vision and Pattern Recognition, San Francisco, CA, USA, 1996, pp. 686–693.
[38] T. Chan, L. Vese, Active contours without edges, IEEE Trans. Image Process. 10 (2) (2001) 266–277.
[39] G. Aubert, P. Kornprobst, Mathematical Problems in Image Processing, Springer Verlag, 2002.
[40] C. Poynton, A Technical Introduction to Digital Video, John Wiley, New York, 1996.